

## ON THE INFERENCE OF DIFFERENTIAL EMISSION MEASURES USING DIAGNOSTIC LINE RATIOS

SCOTT W. MCINTOSH<sup>1</sup>

High Altitude Observatory, National Center for Atmospheric Research,<sup>2</sup> P.O. Box 3000, Boulder, CO 80307-3000; mscott@hao.ucar.edu

Received 1999 September 8; accepted 1999 December 10

### ABSTRACT

Spectroscopic diagnosis of hot optically thin plasmas can be used to infer valuable information about the temperature structure of the emitting plasma volume, through the emission measure differential (DEM) in  $T_e$ ,  $DEM(T_e)$ . However, the uncertainties in atomic parameters (required to model the plasma emission) make such inferences intractable. We demonstrate that it is possible, and relatively straightforward, to implement a formalism and infer  $DEM(T_e)$  in a way such that atomic uncertainties are treated explicitly. Indeed, we show that a hybrid line-ratio/emission-measure method is robust when “standard” inversion methods will fail to produce consistent results.

*Subject headings:* Sun: general — Sun: UV radiation

### 1. INTRODUCTION

The determination of plasma diagnostic distributions, differential emission measures (DEMs), from the observed photons is critical if we are to understand, and assess, the state of the outer solar atmosphere. The data of unprecedented quality provided by the instruments of the NASA/ESA *Solar and Heliospheric Observatory (SOHO)* mission (Fleck, Domingo, & Poland 1995) contain information which can, in principle, allow us to unlock the mysteries of the UV/EUV Sun.

Methods have been in place for decades (see, e.g., Menzel, Aller, & Hebb 1941) that allow us to ascertain estimates of the diagnostic parameters of the solar atmosphere, i.e., the electron density  $n_e$  and temperature  $T_e$ . One such method is the line-ratio approach (see, e.g., Gabriel & Jordan 1972, p. 210; Almlaeky, Brown, & Sweet 1989; Brown et al. 1991; Mason & Monsignori-Fossi 1994 and references therein). This makes use of atomic/ionic structure to predict the ratio of two line emissivities as a function of  $n_e$ ,  $T_e$ , or both. The fact is that this approach yields only a single (often ambiguous) mean measurement, which renders such diagnostics to be of limited use when attempting to analyze the nonequilibrium, inhomogeneous nature of the solar atmosphere.

Another method utilizes the same atomic physics as above, although in a slightly different integral formalism, to characterize the plasma as  $n_e$ ,  $T_e$  (or both) distributions (Brown et al. 1991). This is the more general DEM approach first discussed by Pottasch (1964), but readdressed in the work of Jefferies, Orrall, & Zirker (1972a, 1972b). This approach has a basis depending on a set of rigid assumptions, confining the plasma to a specific, perhaps unrealistic (e.g., Judge et al. 1995), regime. As if this rigidity was not enough, the diagnostic distributions must be inferred numerically as the solutions to ill-posed Fredholm equations of the first kind (Craig & Brown 1976). Such inversions are precarious, that is, they are unstable not only to observational errors (Craig & Brown 1986), but have recently been shown to depend on the accuracy to which we can describe the atomic processes likely to be present (Judge, Hubeny, & Brown 1997). The latter source of error

makes the inverse problem less tractable and definitely requires that such atomic errors are addressed and accounted for appropriately, if any inference of DEMs is to be made from observational data. In this paper we propose a method for doing exactly this.

Recently, in McIntosh, Brown, & Judge (1998), it was shown that both the line-ratio and DEM approaches are, at least mathematically, equivalent. It was also alluded to there that a method bridging the gap and utilizing the best parts of both methods, while alleviating their shortcomings, was a distinct possibility. In this paper we present a method of “ratio inversion” with this purpose in mind.

In § 2 we discuss the mathematical and physical implications of a “ratio inversion” technique (RIT). In § 3 we demonstrate the effectiveness of the approach on a benchmark work in the literature, that of Raymond & Doyle (1981), using data from the Harvard S-055 EUV spectroheliometer (Reeves, Huber, & Timothy 1977) tabulated by Vernazza & Reeves (1978). We demonstrate how well the atomic irregularities discussed by Judge et al. (1997, private communication) are accounted for by our formalism.

### 2. FOUNDATIONS

The total power  $P_i$  radiated by a particular spectral line, labeled  $i$ , emitted by an optically thin volume  $V$  of plasma is given by

$$P_i = \iiint_V h\nu_i A_i n_{u(i)} dV \text{ ergs s}^{-1}, \quad (1)$$

where  $h$  is Planck’s constant,  $\nu_i$  is the frequency of the line,  $A_i$  ( $\text{s}^{-1}$ ) is the Einstein  $A$ -coefficient, and  $n_{u(i)}$  ( $\text{cm}^{-3}$ ) is the population density of the upper level  $u(i)$ . Following standard practice, we define a line emission coefficient,  $K_i[n_e(r), T_e(r)]$ , normalized to the electron density squared as

$$K_i[n_e(r), T_e(r)] = \frac{h\nu_i A_i n_{u(i)}}{4\pi n_e^2} \text{ ergs cm}^3 \text{ sr}^{-1} \text{ s}^{-1}, \quad (2)$$

or as

$$K_i(n_e, T_e) = \frac{h\nu_i A_i}{4\pi} \frac{n_{u(i)}}{n_{\text{ion}} n_e} \frac{n_{\text{el}}}{n_{\text{el}}} \frac{n_{\text{H}}}{n_e} \text{ ergs cm}^3 \text{ sr}^{-1} \text{ s}^{-1}, \quad (3)$$

<sup>1</sup> Also with the Advanced Study Program of the National Center for Atmospheric Research.

<sup>2</sup> The National Center for Atmospheric Research is sponsored by the National Science Foundation.

where  $n_{u(i)}/n_{ion}$ ,  $n_{ion}/n_{el}$ ,  $n_{el}/n_H$ , and  $n_H/n_e$  are the relative population of the upper atomic level of the line, the ionic abundance, elemental abundance, and relative abundance of H to electrons (having a value of 0.8 for the regions of the solar atmosphere considered in this paper), respectively. In principle the first form (eq. [2]) is adequate, but it is instructive to introduce the latter (eq. [3]) to facilitate later discussion.

Using this quantity and realizing that our unit of measurement is the line intensity ( $I_i = P_i/(4\pi S)$  for projected emitting area  $S$ ), we see that

$$I_i = \int_{n_e} \int_{T_e} K_i(n_e, T_e) \mu \times (n_e, T_e) dn_e dT_e \text{ ergs cm}^{-2} \text{ sr}^{-1} \text{ s}^{-1}, \quad (4)$$

where  $\mu(n_e, T_e)$  is the bivariate differential emission measure of Judge et al. (1997) [defined as  $\Psi(n_e, T_e)$  by Brown et al. (1991) with  $\Psi(n_e, T_e) = 4\pi S \mu(n_e, T_e)$ ]. In essence  $\mu(n_e, T_e)$  is a positive definite quantity measuring the volume distribution of emitting plasma differentially as a function of  $n_e$  and  $T_e$  within the plasma, weighted by  $n_e^2$ . From Judge et al. (1997, private communication), the form of  $\mu(n_e, T_e)$  is

$$\mu(n_e, T_e) = \oint_{L_{n_e, T_e}} \frac{n_e^2}{|\nabla n_e| |\nabla T_e| \sin \theta_{n_e, T_e}} dL_{n_e, T_e} \text{ cm}^{-5}, \quad (5)$$

where  $\theta_{n_e, T_e}$  (assumed to be nonzero) is the local angle between vectors  $\nabla n_e$  and  $\nabla T_e$  normal to surfaces  $S_{n_e}$ ,  $S_{T_e}$  of constant electron density and temperature, respectively, and  $L_{n_e, T_e}$  is the line where the constant surfaces meet. The

interested reader is referred to Figure 1 in Brown et al. (1991) for a perspective of the plasma geometry.

At this point we integrate out the electron density dependence (to leave the integral as a function of  $T_e$  only, assuming that we are operating in some fixed  $n_e = n_0$  regime), thus equation (4) becomes

$$I_i = \int_{T_e} K_i(T_e) \xi(T_e) dT_e \text{ ergs cm}^{-2} \text{ sr}^{-1} \text{ s}^{-1}, \quad (6)$$

where

$$\xi(T_e) = \int_{n_e} \mu(n_e, T_e) dn_e \text{ cm}^{-5} \text{ K}^{-1}. \quad (7)$$

We have now introduced the Fredholm equation of the first kind describing the emission measure differential in  $T_e$ , DEM( $T_e$ ), or  $\xi(T_e)$ , (units  $\text{cm}^{-5} \text{K}^{-1}$ ) as it will be designated in symbolic form. Further, to conform with much of the literature, we transform integration variables to  $t_e = \log_{10} T_e$  such that equation (6) becomes

$$I_i = \int_{t_e} K_i(t_e) \xi(t_e) dt_e, \quad (8)$$

where  $\xi(t_e)$  now has units  $\text{cm}^{-5}$ .

The DEM approach is usually posed as an inverse problem requiring the solution of ill-posed<sup>3</sup> integral equations like that of equation (8), of which the effects of numeri-

<sup>3</sup> The degree of ill-posedness is determined by the number of solutions that will adequately fit the data.

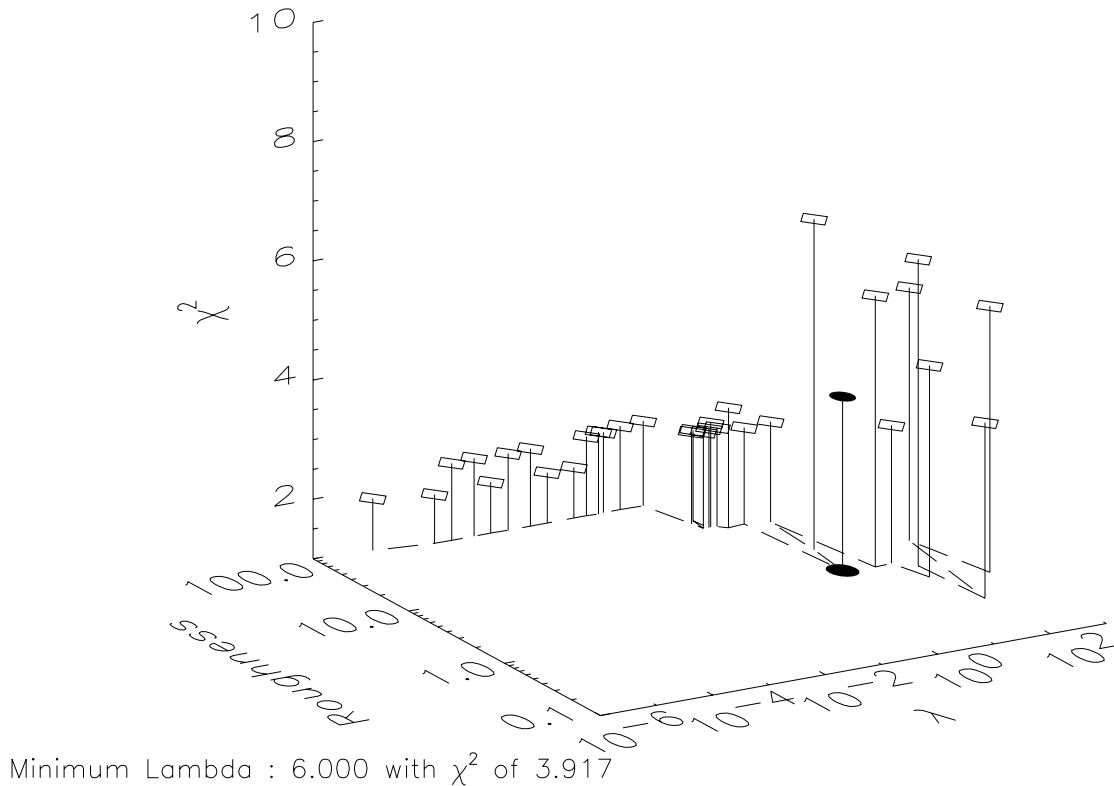


FIG. 1.—The global results of the RIT using a maximum entropy smoothing functional and the set of standard line emission coefficients (kernels). On plotting smoothing parameter  $\lambda$  vs. the roughness of the solution, given above as  $\mathcal{D}^2$  (see eq. [16]) vs.  $\chi^2$  calculated through eq. (15), we are able to identify the value of  $\lambda$  that optimizes the recovery of  $R_{obs}$  with a reasonably smooth function. This value ( $\lambda_{opt}$ ) is determined by finding the point  $\mathbf{v} = \min (\lambda + \mathcal{D}^2 + \chi^2)^{1/2}$  indicated by the filled circle on the upper curve closest to the origin 0. In this case the optimal value of  $\lambda$  ( $\lambda_{opt} = 6$ ) has an associated  $\chi^2$  of 3.917.

cal instability and nonuniqueness are well documented (see, e.g., Craig & Brown 1976).

The form of a typical (discretized over  $M$   $t_e$  points) integral equation once cast as a linear system of equations (see Craig & Brown 1986) is

$$\mathbf{g} = \mathcal{K}\mathbf{f}, \quad (9)$$

where  $\mathbf{g}$ , the  $N$ -element vector of observed data (line intensities in this case), and  $\mathcal{K}$ , the “kernel” ( $N \times M$ ) matrix (containing the atomic parameters, each row containing the emission coefficient of the corresponding element of  $\mathbf{g}$ ) are *known*, and we have to recover  $\mathbf{f}$ , the *unknown* “source” function, or DEM as it is here. As stated above, the possibility that errors are of magnitude  $\geq 15\%$  (Judge et al. 1997) on both sides of equation (9) make this a particularly intractable problem.

The differential emission measure is not the only means to obtain information on the plasma. The “line-ratio” method can be used to evaluate a single estimate of the emitting plasma volume’s temperature. So, consider now two such lines  $i, j$ , where the ratio of the two line intensities is

$$R_{ij} = \frac{I_i}{I_j} = \frac{\int_{t_e} K_i(t_e)\xi(t_e)dt_e}{\int_{t_e} K_j(t_e)\xi(t_e)dt_e}, \quad (10)$$

and if the emission coefficients are different, then the ratio depends on  $t_e$ . If the plasma is homogeneous in temperature, i.e., isothermal, we could express the  $\xi(t_e)$  as  $\xi(t_e) = \xi_0 \delta(t_e - \langle t_e \rangle)$  such that, on substituting this expression into equation (10) and integrating over the whole temperature domain, we have

$$R_{ij} = \frac{\xi_0 K_i(\langle t_e \rangle)}{\xi_0 K_j(\langle t_e \rangle)}, \quad (11)$$

and for the particular line pair  $i, j$  we may express  $R_{ij}$  in terms of the “mean” spectroscopic temperature,  $\langle t_e \rangle_{ij}$ ,

$$R_{ij} = \frac{K_i(\langle t_e \rangle)}{K_j(\langle t_e \rangle)}. \quad (12)$$

From equation (12) it is trivial<sup>4</sup> to evaluate the “mean” spectroscopic temperature of the emitting plasma,  $\langle t_e \rangle_{ij}$ , essentially the temperature of an isothermal plasma that would produce the identical intensity ratio. It should be clear that different ratios will produce different values of  $\langle t_e \rangle$ . Distributions can be built, but in a different fashion than the DEM.

The DEM inversion intractability can be simply circumvented if the dominant errors in the line emission coefficients are systematic, as suggested by Judge et al. (1997). In fact, the line-ratio method described above can explicitly deal with some of the systematic errors, since the ratio of two quantities with the same systematic error (say, two lines from the same ionic species or even isoelectronic sequence) will be largely filtered out by taking the ratio of those terms.<sup>5</sup> The question, then, is can we formulate a line-ratio-like methodology to infer  $\zeta(T_e)$ ?

<sup>4</sup> Assuming a monotonic dependence of  $R_{ij}$  on  $t_e$ .

<sup>5</sup> With a constant DEM the effect of such systematic errors can be filtered out completely. When the DEM is not constant, the true situation, the differences in variability of the functions involved (DEM and line emissivities) will be critical in helping to determine the cancellation of the errors.

## 2.1. The Ratio Inversion Technique (RIT)

The nonlinearity required to solve equation (10) and the need to incorporate a measure of error in the atomic parameters used requires that we seek a new method to solve for  $\xi(t_e)$  using a line-ratio formalism. Consider, then, the set of  $N$  line ratios  $\{R_{ij}\}$ . We have for line pairs  $i, j$  (and  $i \neq j$ ), with respective integrated line intensities  $I_i$  and  $I_j$ ,

$$R_{ij} = \frac{I_i}{I_j} = \frac{\int_{t_e} K_i(t_e)\xi(t_e)dt_e}{\int_{t_e} K_j(t_e)\xi(t_e)dt_e}, \quad (13)$$

and we wish to “solve” a system of  $N$  such equations ( $N$  line pairs) for  $\xi(t_e)$ .

In an ideal world, one where the solution to equation (13) is a smooth positive definite function of  $t_e$ , we would seek the form of  $\xi(t_e)$  satisfying the least-squares expression,

$$X^2(R_{\text{obs}}, R_{\text{calc}}) = \sum_{l=1}^N \left[ \frac{(R_{\text{obs}}^l - R_{\text{calc}}^l)^2}{\sigma_{l_{\text{obs}}}^2 + \sigma_{l_{\text{calc}}}^2} \right] \approx 1, \quad (14)$$

where  $l$  is the label of a particular line pair,  $\{R_{\text{obs}}\}$  is the set of observed optically thin line ratios with errors  $\sigma_{l_{\text{obs}}}$ , theoretical estimates of the errors in the relevant atomic parameters [in  $K_i(t_e)$  and  $K_j(t_e)$ ] are given by  $\sigma_{l_{\text{th}}}$  (discussed in § 2.3), and the set of  $\{R_{\text{calc}}\}$  are calculated using equation (13). However, as is the case with all ill-posed inverse problems, we must seek some form of regularized solution for  $\xi(t_e)$  that minimizes equation (14) subject to some criterion, e.g.,

$$\chi^2 = X^2(R_{\text{obs}}, R_{\text{calc}}) + \lambda \Phi[\xi(t_e)] \quad (15)$$

(adopting  $X$ , above, to be a form of the statistical  $\chi^2$  measure between  $R_{\text{obs}}$  and  $R_{\text{calc}}$ ), where  $\lambda$  and  $\Phi[\xi(t_e)]$  are the smoothing parameter and smoothing functional, respectively. The choice of  $\Phi[\xi(t_e)]$  is subjective and is chosen to reflect the nature of the solution space (see Craig & Brown 1986). For example, if we were to assume that  $\xi(t_e)$  is smooth to the  $n$ th polynomial order, then we would choose

$$\Phi[\xi(t_e)] = \left| \int_{t_e} \frac{d^n \xi(t_e)}{dt_e^n} \right|^2 dt_e, \quad (16)$$

where  $\xi(t_e)$  will clearly be a discretized function and we will be required to calculate equation (16) as a forward finite-difference estimate of the actual integral. Of course, equation (16) can be placed on a general footing [making no assumption about the functional form of  $\xi(t_e)$ ] by employing a maximum entropy (ME) measure like

$$\Phi[\xi(t_e)] = \int_{t_e} \frac{\xi(t_e)}{f(t_e)} \log \left[ \frac{\xi(t_e)}{f(t_e)} \right] dt_e, \quad (17)$$

for some (usually flat) prior function  $f(t_e)$ . The analysis presented in § 3 will use this ME smoothing because of its unbiased nature and the ensurance of positivity, i.e., the solution will represent the physical solution best fitting the data and not some member of the family of  $n$ th degree smooth curves; clearly a more suitable situation.

Digressing a little, Fludra & Schmelz (1995) employed a line-ratio approach loosely comparable to the RIT to infer coronal atomic abundances of the flaring coronal plasma. Their discussion focused on the analysis of soft X-ray (10–100 keV) lines obtained by the *Solar Maximum Mission* (SMM) flat crystal spectrometer (FCS) (Acton et al. 1980) and produced, as a by-product, DEM functions  $\xi(t_e)$  for the

high-temperature ( $6 \leq t_e \leq 8$ ) flaring plasma. The analysis Fludra & Schmelz (1995) presented, however, did not attempt to compensate for the potentially damaging theoretical atomic uncertainties discussed above. Even though the community was well aware of the difficulties of constructing reliable atomic transition models (Jordan 1974), the topic was not readdressed until the work of Judge et al. (1997).

The form of equation (13) means that we cannot use standard Tichonov regularization methods (imposing smoothing like eq. [16]), but that we must adopt a new nonlinear approach.<sup>6</sup> To this end we have chosen a genetic algorithm (GA) because of its numerical robustness (Goldberg 1989) and the ease with which nonlinear calculations like equation (15) can be encoded (Charbonneau 1995). For the calculations presented here we will specify the  $t_e$  mesh over which the integrals are discretized and use the ME smoothing functional (over a wide range of values for  $\lambda$ ) to analyze the numerical stability of the solutions obtained. Indeed we show that for the test chosen the results are conclusive that the RIT is not influenced greatly by large systematic errors in the atomic ionization/recombination rate coefficients that could make the results of standard intensity inversions highly ambiguous. *That is, the RIT is insensitive to errors that are likely to dominate standard inversion procedures and, therefore, provides a new means of obtaining less ambiguous results about the emitting optically thin region of the solar atmosphere under examination.*

## 2.2. Implementation of the RIT

As noted above we are making use of the adaptability of a GA to perform this nonlinear inversion (see Press et al. 1992).<sup>7</sup> The GA approach allows a high degree of user control and also effectively allows us to specify the number of generations (10,000) over which the solution will evolve; the final solution being that which best optimizes equation (15). In addition, the GA method we use implements a genetic precedence operator known as “elitism,” its function being that the “best” solution at the end of each generation is retained in the population of possible solutions for “breeding” of the next and preceding generations (until superseded; see, e.g., Charbonneau 1995 for a concise description of the genetic operators used here).

Each individual in the population, composed of 100 individuals, is made up of  $M = 30$  “parameters” with the  $i$ th parameter evaluating the DEM function at the  $i$ th point in  $t_e$  space, i.e.,  $\xi(t_{ei})$ . RIT does not couple these parameters (there is no interpolation between them), and the choice of  $M = 30$  as the number of discretization points is entirely arbitrary. This number can be increased, but care must be exercised because, as  $M$  increases, the line emissivities get “closer” to the continuous integral operators<sup>8</sup> they represent and increase the possibility of numerical instability. The choice of  $N$ , the number of line ratio pairs used in the

<sup>6</sup> Standard linear inversion techniques are not valid because eq. (13) contains the optimizing quantity on numerator and denominator of a calculation and the resulting ratio of linear systems is mathematically meaningless, as stated above.

<sup>7</sup> We note that other optimization methods may be able to solve this system of equations, see, e.g., AMOEBA-A “downhill” SIMPLEX algorithm from Press et al. (1992).

<sup>8</sup> Not only do they approach the actual form of the integral operators, a patently poor property, but they reduce the effectiveness of the genetic operators; this is discussed as earlier, see, e.g., Goldberg (1989).

analysis, is also arbitrary, but any significant increase in  $N$ , say above 30, may also produce an increase in numerical instability of the recovered solution. This is particularly true if using an increased number of ratio pairs from one particular ionic stage, since then the “linear dependence” of the operator to be inverted is increased considerably; see discussion in McIntosh, Charbonneau, & Brown (2000).

The action of the RIT is best described as the following:

1. Generate 100 random solutions as an initial population, calculate the resulting  $\chi^2$  of equation (15) for each individual.
2. Choose a subset according to their values of  $\chi^2$  and breed them to produce a new population.
3. Calculate the value of  $\chi^2$  for each individual in the new population.
4. Replace the old population with the new one.
5. Check that the number of generations has reached its maximum value; if not, return to step 2.

Our work is not finished on the recovery of a solution from the RIT. The recovered function  $\xi(t_e)$  from optimizing equation (15) (via eq. [14]) does not allow us to fix the amplitude of  $\xi(t_e)$ . This is simply because the inferred solution will always be a scalar multiple  $\mathcal{C}$  of its true value since

$$R_{\text{calc}} = \frac{\int_{t_e} K_i(t_e)[\mathcal{C}\xi(t_e)]dt_e}{\int_{t_e} K_j(t_e)[\mathcal{C}\xi(t_e)]dt_e} \quad (18)$$

will always hold. So, to resolve this problem we must use the inferred solution  $\xi(t_e)$  to recalculate the  $N$  line intensities,  $I_{\text{calc}}$ . We choose the scaling factor  $\mathcal{S} (\approx \mathcal{C})$  given by

$$\mathcal{S} = \frac{1}{\sum_{j=1}^N w_j} \left[ \sum_{j=1}^N w_j \left( \frac{I_{\text{obs}}^j}{I_{\text{calc}}^j} \right) \right], \quad (19)$$

where  $w_j = 1/\sigma_{\text{obs}}^j$  for observational error  $\sigma_{\text{obs}}^j$ . In practice, we need only fix a single line intensity in the calculation to fix the absolute magnitude of  $\xi(t_e)$ , but in the presence of noise this leads to an element of bias in the function scaling. This possible source of bias arises since any particular line intensity is only “sensitive” over a short span of the whole  $t_e$  domain (from the  $t_e$  dependence of the line emission coefficient); the concept of “emissivity coverage” is discussed at length in McIntosh et al. (2000). Thus, equation (19) yields an unbiased scaling factor for  $\xi(t_e)$  by effectively averaging out the scaling over the entire  $t_e$  domain and weighting according to the observational errors.

## 2.3. The Calculation of Atomic Errors

To calculate meaningful values of  $\sigma_{\text{th}}$  (for each line pair  $l$ , see eq. [14]), we have performed a Monte Carlo simulation to get a distribution of 20 perturbed line emissivities for each transition. Perturbed, in the sense that their component atomic terms (rates and coefficients) are randomly perturbed about their “accepted” values. The amounts by which these coefficients and rates are perturbed are relevant to figures put forward in the literature, specifically in Judge et al. (1995) and Judge et al. (1997). An analog to equation (3) will help with this discussion, i.e., we can express the emissivity of the optically thin emission line  $i$  (in the simplest sense) as

$$K_i(t_e) \approx \kappa \times \mathcal{X}_i(t_e) \times \mathcal{Y}_i(t_e), \quad (20)$$

where  $\kappa$  is a constant,  $\mathcal{X}_i(t_e) = n_{\text{ion}}/n_{\text{el}}$  is the conglomerate of the bound-free (b-f) terms, and  $\mathcal{Y}_i(t_e) = n_{u(i)}/n_{\text{ion}}$  of the

bound-bound (b-b) terms of the transition as functions of  $t_e$ , respectively. So, if these quantities have associated errors  $\delta x_i$  and  $\delta y_i$ , then the fractional error in the line emissivity can be expressed as<sup>9</sup>

$$\left(\frac{\delta K_i}{K_i}\right)^2 = \left(\frac{\delta x_i}{x_i}\right)^2 + \left(\frac{\delta y_i}{y_i}\right)^2. \quad (21)$$

The calculations presented in this chapter have associated standard ( $1\sigma$ ) deviations in the fractional errors that are set as follows (see Judge et al. 1997):

1. For the bound-bound processes we adopt a value of 3%. This of course ensures, by definition, that 32% of the random realizations will have errors in excess of 3%.

2. We have chosen to use logarithmic (base 10; log-normal distributed) deviations of  $\pm 0.1$  about the mean value for bound-free processes. This value is clearly an estimate, because the amplitude of errors in such (b-f) processes are not well known, Judge (1997, private communication). These values reflect possible lower magnitude limits on the b-b and b-f terms. So, the effects on line emissivity  $K_i(t_e)$  are conservatively estimated to lie between 10% and 125%, respectively.

The actual process of perturbing the atomic rates/coefficients is carried out by routines of the HAOS-Diaper atomic calculation package (Judge & Meisner 1994). To obtain actual estimates of  $\sigma_{\text{th}}$  we have to obtain a distribution of line emissivities for each line, each with different random realizations of the constituent atomic factors. We obtain 20 such realizations for each line and use the following recipe to construct values of  $\sigma_{\text{th}}$  for the line pair  $l = (i, j)$ .

1. Calculate the integrated line intensities for each line and each perturbed line emissivity; yielding a distribution of  $Q = 20$  line intensities. It should be noted that we use a constant (i.e., flat)  $\xi_0(t_e)$  to calculate these intensities, but such an approximation is not taken lightly and is made primarily to have a simple and uniform error estimate for

every line no matter at what temperature it is formed at. So, returning to the problem in hand we have calculated 20 randomly perturbed values  $I_i$  (see eq. [8]),

$$I_i = \int_{t_e} K_i(t_e) \xi_0(t_e) dt_e. \quad (22)$$

2. Repeat the previous calculation for every possible line until distributions of line intensities  $I_i = \{I_i^1, \dots, I_i^Q\}$  are formed.

3. Use the distributions of step 2 to form distributions for the various emission line pairs  $R_l = \{R_l^1, \dots, R_l^Q\}$ . Note that the individual values of  $R_l^j (1 \leq j \leq Q)$  are calculated with the denominator, and numerator line intensities are taken from the same model,  $j$ .

4. Given that we now have random distributions for the same “flat”  $\xi(t_e)$  function, it is reasonable to assume that the standard deviations ( $1\sigma$ ) of the distributions well approximate the values of  $\sigma_{\text{th}}$  (see the values given in Table 1).

### 3. RESULTS : RIT APPLICATION TO SKYLAB S-055 SPECTROHELIOMETER DATA

In this section we make use of the composite (average) quiet-Sun spectra of Vernazza & Reeves (1978; Figs. 2–4) observed in the 280–1350 Å wavelength range of the Harvard S-055 spectroheliometer (Reeves et al. 1977) on the Apollo Telescope Mount during the 1973–74 *SkyLab* mission. It is our aim to make use of the 39 strongest first-order lines (see Table 1) to infer an average quiet Sun  $\xi(t_e)$  and make a comparison to those obtained using a standard intensity inversion (both calculated using perturbed and standard<sup>10</sup> kernels) and the benchmark form published by Raymond & Doyle (1981). In this study we are careful to

<sup>9</sup> Judge et al. (1997) erroneously used the linear form. Eq. (21) is the correct form.

<sup>10</sup> “Standard” in this sense means calculated using coefficients that are the accepted values in the atomic calculations.

TABLE 1  
DETAILS OF THE LINE-RATIO PAIRS USED IN THE RIT CALCULATIONS

Number	Ion <sub>N</sub>	$\lambda_N$ (Å)	Ion <sub>D</sub>	$\lambda_D$ (Å)	$\sigma_{\text{th}}/R_{\text{th}}$	Number	Ion <sub>N</sub>	$\lambda_N$ (Å)	Ion <sub>D</sub>	$\lambda_D$ (Å)	$\sigma_{\text{th}}/R_{\text{th}}$
1	C II	903.962	C II	1037.02	0.0386	2	C II	1037.02	C II	1335.66	0.0481
3	C III	977.017	C III	1175.71	0.0264	4	Mg VIII	430.465	Mg VIII	436.670	0.0355
5	Mg X	609.793	Mg X	624.941	0.0013	6	Ne VI	401.136	Ne VI	558.594	0.0567
7	Ne VI	401.136	Ne VI	562.701	0.0570	8	N III	685.817	N III	989.799	0.0511
9	N III	685.817	N III	991.511	0.0506	10	O II	718.505	O II	833.330	0.2422
11	O III	525.797	O III	702.332	0.0521	12	O IV	553.329	O IV	790.199	0.0379
13	O IV	553.329	O IV	787.710	0.0368	14	C II	1037.02	C III	977.017	0.2282
15	Mg X	609.793	Mg IX	368.070	0.5075	16	Ne VI	562.701	Ne VII	465.219	0.0864
17	Ne VII	465.219	Ne VIII	770.409	0.1597	18	Si II	1264.74	Si III	1206.50	0.1148
19	N II	1085.53	N III	685.817	0.2122	20	O III	599.598	O II	834.465	0.0496
21	O III	702.332	O II	834.465	0.0398	22	O II	718.505	O III	525.797	0.2634
23	O IV	790.199	O III	702.332	0.1684	24	O IV	553.329	O V	629.730	0.0613
25	O IV	553.329	O V	758.675	0.0578	26	O V	629.730	O VI	1031.91	0.2696
27	O II	833.330	C III	977.017	0.1260	28	N V	1238.82	O IV	787.710	0.1556
29	Si XII	499.406	Fe XV	417.258	0.3568	30	Si XII	520.665	Fe XV	417.258	0.3552

NOTE.—Listed are the ratio pair number, the numerator and denominator (subscript  $N$  and  $D$  quantities, respectively) atom, ionization stage, wavelengths, and the ratio of standard deviation,  $\sigma_{\text{th}}$ , to the theoretical line ratio,  $R_{\text{th}}$ , from the ensemble of 20 calculations for ratio pair  $l$ . It is easy to identify pairs with large errors.

include the emissivities from lines (particularly of the same ionic multiplets) that form blends with those lines identified within the spectral resolution of the instrument (1.6 Å FWHM), in addition to those blends noted in the tables of Vernazza & Reeves (1978). We then find that some 87 emissivities combine linearly to form the 39 used in the present analysis.

In the following we use kernels (standard and perturbed) calculated (using the aforementioned HAOS-Diaper package) for a constant electron pressure, derived from the same data by Raymond & Doyle (1981),  $4 \times 10^{14} \text{cm}^{-3} \text{K}$ . The assumption of constant  $P_e$  is not only to make comparison with the calculations of Raymond & Doyle (1981) but to ensure that the calculations are consistent with observations and currently accepted models of the solar transition region (TR), which suggest that the TR is a constant pressure interface between the chromosphere and corona (see, e.g., chap. 6 of Mariska [1992]). In addition we are limiting the number of  $t_e$  discretization points to  $M = 30$  (primarily for the reasons mentioned in § 2.2) over the range  $4.0 \leq t_e \leq 6.5$ . We use both standard and perturbed kernels (with the latter belonging to a single randomly selected set of § 2.3) to test the hypothesis that the RIT is robust to potential atomic inaccuracies as alluded to in McIntosh et al. (1998) and to recover a structure similar to that of Raymond & Doyle (1981). Indeed, performing such ratio inversions is a worthwhile exercise, especially when we consider the insufficiency of standard inversion techniques in dealing with such inaccuracies.

As mentioned in § 2.1 the RIT optimizes equation (15), where the quantities are as previously defined and  $\Phi[\xi(t_e)]$  is defined by the logarithmic smoothing operator of equa-

tion (17). We obtain results for a range of values for  $\lambda$  ( $10^{-4}$ ,  $10^2$ ) for both standard (Fig. 1) and perturbed (Fig. 2) kernels.

In each of Figures 1 and 2 the means by which we identify the best solution is simple: in any inverse formalism it is standard practise to plot  $\chi^2$  against  $\lambda$  and choose the best solution as that with  $\lambda$  closest to the origin of the plot, according to  $(\chi^2 + \lambda^2)^{1/2}$  (see, e.g., Turchin, Kaslov, & Malkevich 1971). The addition of the GA method in the RIT adds an extra degree of freedom in the calculation, i.e., we need to find a solution that is sufficiently smooth; to this end we have plotted  $\chi^2$  against  $\lambda$  against roughness in Figures 1 and 2. We evaluate the roughness ( $\mathcal{D}$ ) of any test solution as

$$\mathcal{D} = |\Phi[\xi(t_e)]|, \quad (23)$$

where  $\Phi[\xi(t_e)]$  is given, in this case, by equation (17). In Figures 1 and 2 the location of the best solution is indicated by a solid black circle according to the minimal value of  $(\chi^2 + \lambda^2 + \mathcal{D}^2)^{1/2}$ .

Figures 3 and 4 show the details of the best solutions indicated in Figures 1 and 2, respectively. Figure 3a shows the optimal solution for the RIT (*solid line*), the intensity inversion for the same data (*dashed line*; 39 emission lines used) and the quiet-Sun average DEM presented by Raymond & Doyle (1981) for this data set (*triple-dot-dashed line*). These inversions are for the standard kernels. The intensity inversion shown is that which produces a comparable fit to the line ratios used in the calculation, the error bars on this and the RIT solution are calculated a posteriori relative to the discrepancies between the observed and calculated line ratios. The bottom portion of Figure 3 exhibits

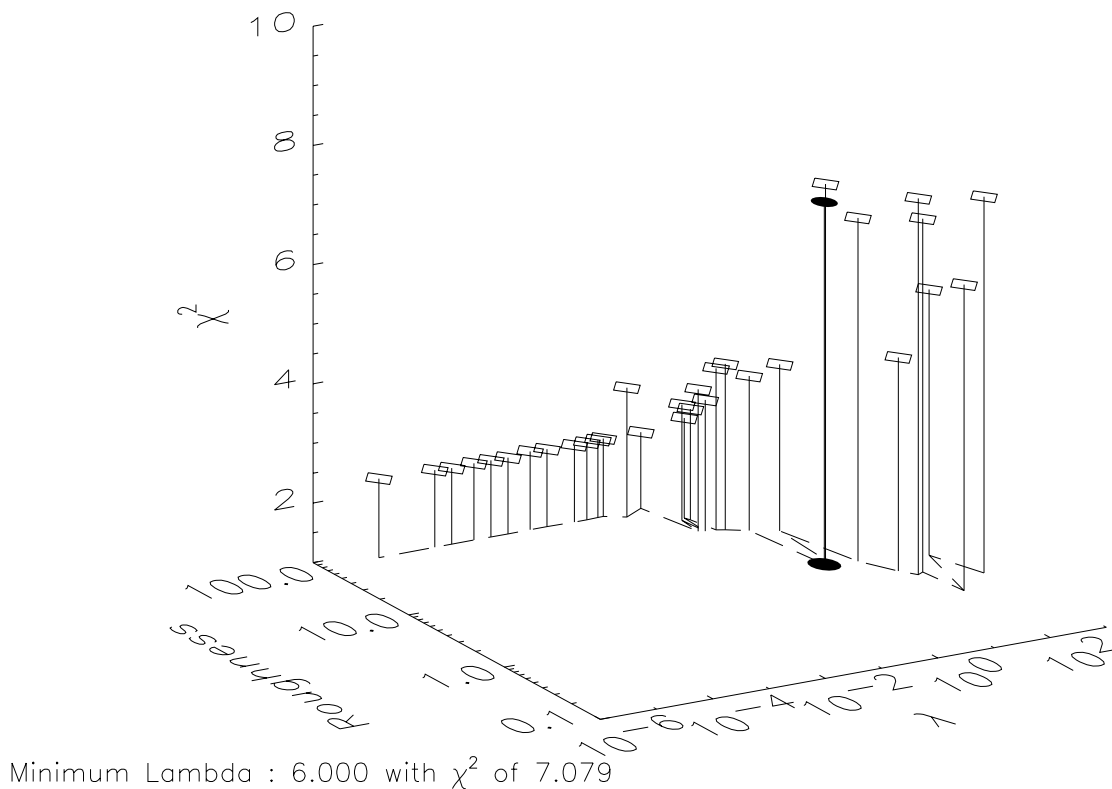


FIG. 2.—Global results of the RIT using a maximum entropy smoothing functional and the set of perturbed line emission coefficients (kernels). See Fig. 1 for further details. In this case the optimal value of  $\lambda$  ( $\lambda_{\text{opt}} = 6$ ) has an associated  $\chi^2$  of 7.079.

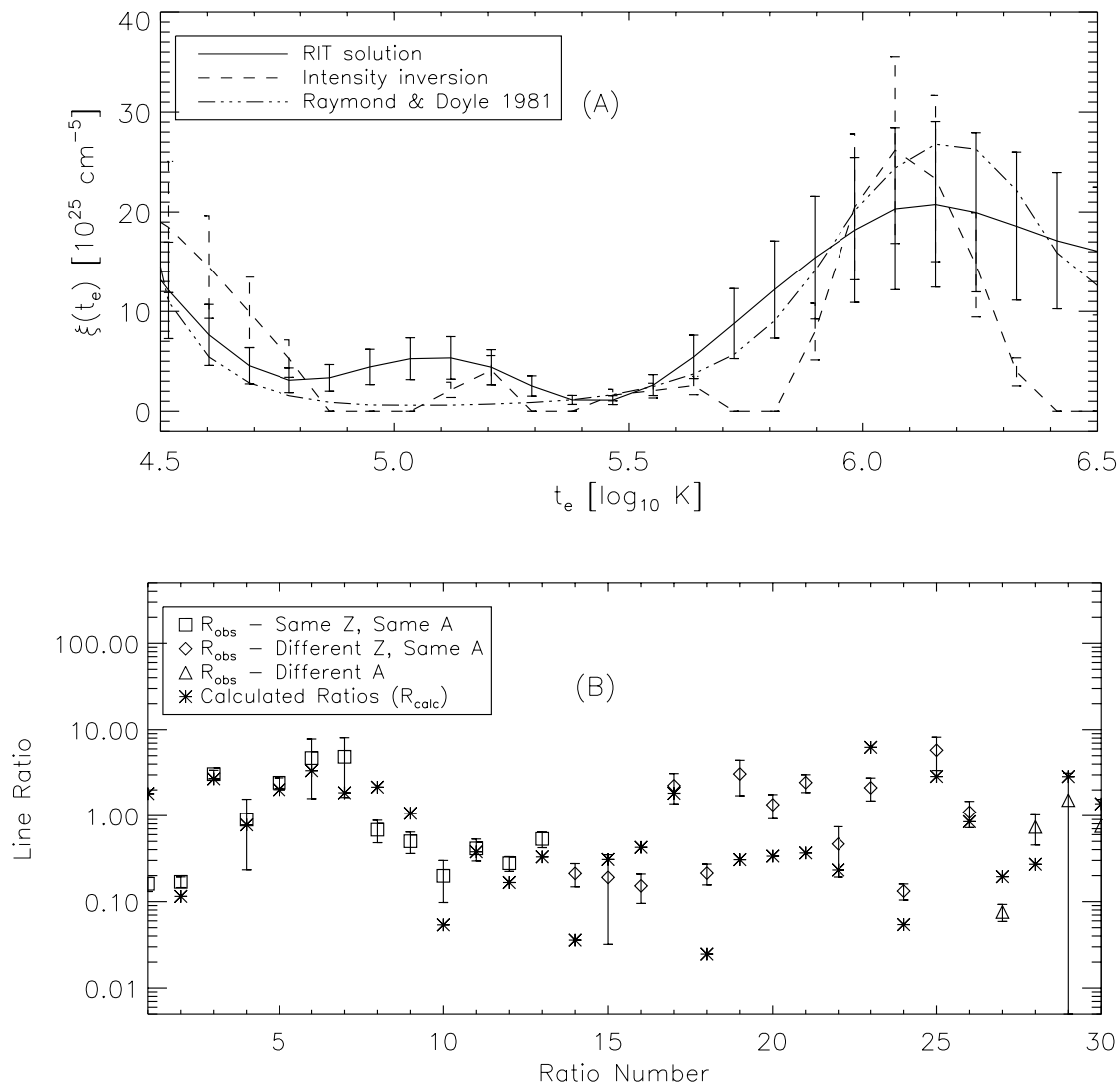


FIG. 3.— (a): Optimal ( $\lambda_{\text{opt}} = 6$ ) solution for the RIT with standard kernels (solid line) indicated in Fig. 1. Also shown is the solution for a line intensity inversion (dashed line) and that calculated by Raymond & Doyle (1981) for the same line intensities. (b) demonstrates the accuracy to which the observed line ratios were recovered by the inferred RIT  $\xi(t_e)$  (asterisks) within the observational errors. The legend of panel (b) is labeled according to the ratio type: same atom,  $A$ , and same ionization stage,  $Z$ , ratios are shown as squares, while different  $Z$ , same  $A$  ratios and different  $A$  ratios are shown as diamonds and triangles, respectively.

this discrepancy for the RIT solution. In this case the value of  $\chi^2$  was 3.917.

In Figure 4 we show an identical plot for the perturbed kernels. Here, the optimal solution has  $\chi^2$  of 7.079. Values greater than 1 indicate that we have underestimated the denominator of equation (14), not a surprising result since the errors in the atomic data are actually unknown. It is also worth noting that the solution (for both “standard” and “perturbed” kernels) gives rise to large discrepancies between the calculated and observed ratios for lines of the same atom, but different ionization stage (diamond).

On inspection of Figures 3 and 4 it is clear that (within the error bars) there is very little functional difference between the RIT solutions, yet the intensity inversion solutions have functional variations far outside the range permitted by the error bars. In short, the solution returned by the RIT is much less sensitive to the errors in the atomic calculations since it produces a quantitatively identical solution in both cases, whereas the intensity inversions

functional form varies a great deal depending on the kernels used.

### 3.1. RIT versus Intensity Inversion : $A$ “Forward-Backward” Comparison

To test the hypothesis that the RIT provides a more robust inference of  $\xi(t_e)$ , we will make a “forward-backward” comparison between the RIT and a standard inversion technique<sup>11</sup> (see, e.g., Thompson 1991; Griffiths & Jordan 1998; Landi & Landini 1998); both using ME smoothing. Again, these inversions make use of  $P = 30$  discretization points uniformly distributed in  $t_e$ . The forward calculation involves computation of line intensities (with uniformly distributed errors in the range  $\pm 15\%$ ) for a given model  $\xi(t_e)$  function. Again, as above, the model we have

<sup>11</sup> Standard, but not to be confused with the forward solution methods extensively used.

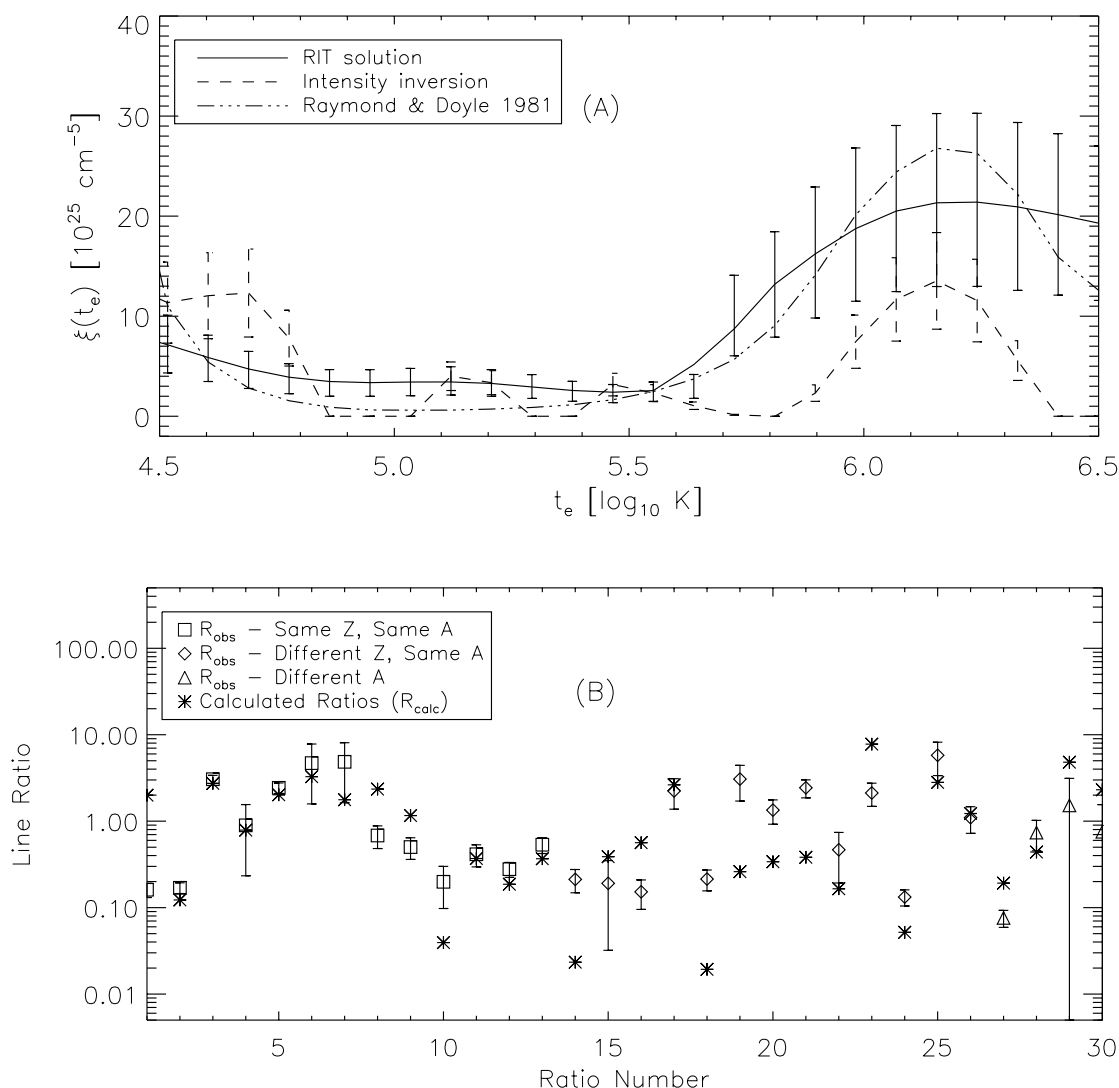


FIG. 4.—(a) Optimal ( $\lambda_{\text{opt}} = 6$ ) solution for the RIT with perturbed kernels (*solid line*) indicated in Fig. 1. Also shown is the solution for a line intensity inversion (*dashed line*) and that calculated by Raymond & Doyle (1981) for the same line intensities. In comparison with Fig. 3 it is clear that the RIT solutions have a characteristic functional form that is the same, within the error bars, but the intensity inversions do not behave in nearly the same way. (b) The plot demonstrates the accuracy to which the observed line ratios were recovered by the inferred RIT  $\xi(t_e)$  (*asterisks*) within the observational errors; the legend is labeled with the same conventions as Fig. 3b.

used is the average quiet Sun  $\xi(t_e)$  taken from Figure 3 of Raymond & Doyle (1981).<sup>12</sup>

The results of the forward-backward calculations are shown in Figure 5. The solid line identifies the RIT solution and dashed line is the intensity inversion solution. Both of these solutions give intensity recoveries with  $\chi^2 \approx 1.5$  and, hence, are judged equivalent solutions on that criteria alone. In Figure 5a we see that both recover  $\xi(t_e)$  well, but this is no great surprise given that the standard emissivities were used in the forward calculation of the intensities used. Figure 5b demonstrates the benefit gained in using the RIT: now the solution for the intensity inversion is not only numerically unstable, but zero in parts, and this is with a

<sup>12</sup> We have used the numbers from Fig. 3 of Raymond & Doyle (1981) and interpolated a best fit curve to the points. This curve is then our model  $\xi(t_e)$  and is used to compute synthetic line intensities for the 39 lines by computing eq. (8) for each. Such calculations are termed as “forward” calculations, using the RHS of eq. (8) to determine the LHS. The model curve of Raymond & Doyle (1981) is then the target function of the “backward,” or inverse, process.

relatively high value of  $\lambda$ . In general, it is clear that the RIT solution is significantly better. To obtain a better recovery of  $\xi(t_e)$  with the intensity inversion requires that we increase  $\lambda$  significantly, see McIntosh et al. (2000) for further discussion.

#### 4. POSSIBLE EXTENSION OF THE RIT

In principle the extension of the RIT code as it stands to deal with DEM in  $n_e$  [ $\xi(n_e)$ ] (see Almlaeky et al. 1989; Brown et al. 1991; McIntosh 1998) or the bivariate DEM (i.e., of  $n_e$  and  $T_e$ ;  $\mu(n_e, T_e)$ , see eq. [4]) of Hubeny & Judge (1995) is numerically very straightforward, although the latter will be significantly more computationally expensive. A work in progress incorporating both  $n_e$  and  $t_e$  allowing us to target some integral equation in  $p_e$  (an analog to eq. [4]) would address some of the ambiguity and consistency problems of treating constant  $t_e$ , constant  $n_e$  problems individually (McIntosh 2000). Indeed, such an approach may bypass the problems of the full bivariate inversion raised by Judge et al. (1997). In addition to these extensions, the

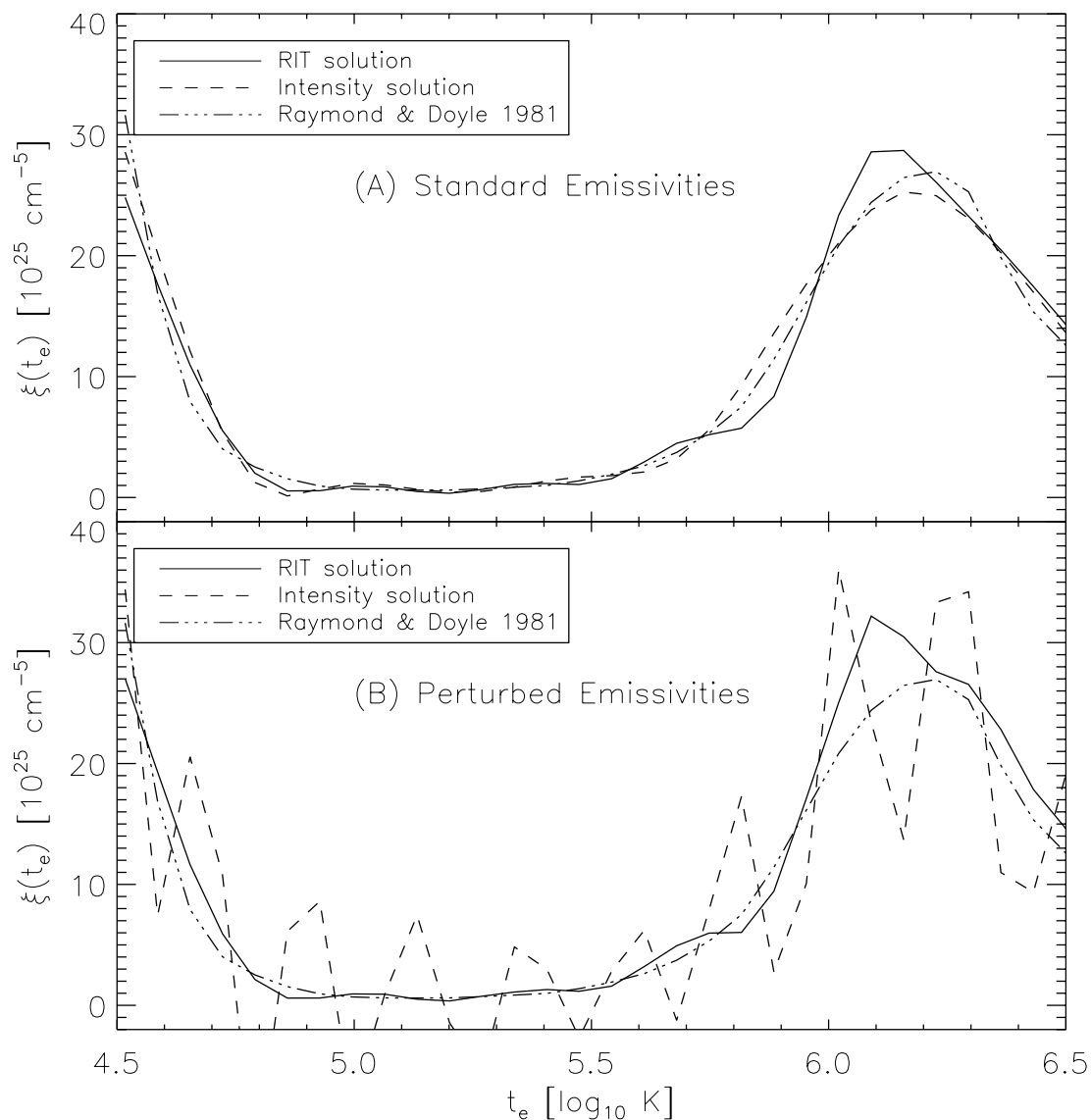


FIG. 5.—The results of the “forward-backward” calculation using line intensities calculated by putting the Raymond & Doyle (1981)  $\xi(t_e)$  function into the right-hand side of eq. (8). In both panels we show the reconstructed  $\xi(t_e)$  functions for RIT (solid line;  $\lambda = 4$ ) and a standard intensity inversion (dashed line;  $\lambda = 10^3$ ) for both standard (panel a) and perturbed (panel b) emissivities. The forward calculation was performed using the standard emissivities, so the fact that both methods recover the source  $\xi(t_e)$  well in panel (a) is no surprise. From panel (b) it is clear that the RIT is better equipped to deal with the perturbations in the line emissivities. Indeed, the RIT solution is numerically stable and physical (positive definite), whereas the intensity inversion is neither.

application of the RIT may shed light on cases where basic assumptions underlying the DEM inverse problem are partially violated, e.g., ionization equilibrium or thermalized particle distributions. This, however, is a subject for further work.

### 5. CONCLUSION

We have demonstrated that it is possible to develop and utilize a line-ratio-like methodology to infer DEMs in  $t_e$ ,  $\xi(t_e)$ , in a numerically robust manner. In addition, RIT is able to address and overcome difficulties presented by

uncertainties in atomic parameters discussed by Judge et al. (1997) [allbeit for the case of  $\mu(n_e, T_e)$ ] as being a “fundamental limitation” in the inference of DEMs from remotely sensed data.

The author is grateful for the interesting comments made on this text by C. Jordan, P. Judge, and P. Charbonneau and acknowledges the support of a UK PPARC studentship and the HAO visitor program during which this research was carried out.

### REFERENCES

- Acton, L. W., et al. 1980, *Sol. Phys.*, 65, 53  
 Almlaeky, Y. M., Brown, J. C., & Sweet, P. A. 1989, *A&A*, 224, 328  
 Brown, J. C., Dwivedi, B. N., Sweet, P. A., & Almlaeky, Y. M. 1991, *A&A*, 249, 277  
 Charbonneau, P. 1995, *ApJS*, 101, 309  
 Craig, I. J. D., & Brown, J. C. 1976, *A&A*, 49, 239  
 ———. 1986, *Inverse Problems in Astronomy: A Guide to Inversion Strategies of Remotely Sensed Data* (Bristol: Hilger)  
 Fleck, B., Domingo, V., & Poland, A. I. 1995, *The SOHO Mission* (Dordrecht: Kluwer)  
 Fludra, A., & Schmelz, J. T. 1995, *ApJ*, 447, 936  
 Gabriel, A. H., & Jordan, C. 1972, *Case Studies in Atomic Collision Physics*, ed. E. McDaniel & M. C. McDowell (Holland: elsevier North), chap. 4  
 Goldberg, D. A. 1989, *Genetic Algorithms in Search of Optimization and Machine Learning* (New York: Wesley)

- Griffiths, N. W., & Jordan, C. 1998, *ApJ*, 497, 883  
Hubeny, V., & Judge, P. G. 1995, *ApJ*, 448, L61  
Jefferies, J. T., Orrall, F. Q., & Zirker, J. B. 1972a, *Sol. Phys.*, 22, 307  
———. 1972b, *Sol. Phys.*, 22, 317  
Jordan, C. 1974, *A&A*, 34, 69  
Judge, P. G., Hubeny, V., & Brown, J. C. 1997, *ApJ*, 475, 275  
Judge, P. G., & Meisner, R. 1994, in *The Third SOHO Workshop, Solar Dynamic Phenomena and Solar Wind Consequences*, ed. J. J. Hunt (ESA SP-373; Noordwijk: ESTEC), 67  
Judge, P. G., Woods, T. N., Brekke, P., & Rottman, G. J. 1995, *ApJ*, 455, L85  
Landi, E., & Landini, M. 1998, *A&AS*, 133, 411  
Mariska, J. T. 1992, *The Solar Transition Region* (Cambridge: Cambridge Univ. Press)  
Mason, H. E., & Monsignori-Fossi, B. C. 1994, *A&A Rev.*, 6, 123  
McIntosh, S. W. 1998, Ph.D. thesis, Univ. of Glasgow  
McIntosh, S. W. 2000, in preparation  
McIntosh, S. W., Brown, J. C., & Judge, P. G. 1998, *A&A*, 333, 333  
McIntosh, S. W., Charbonneau, P., & Brown, J. C. 2000, *ApJ*, 529, 1115  
Menzel, D. H., Aller, L. H., & Hebb, M. H. 1941, *ApJ*, 93, 230  
Pottasch, S. R. 1964, *Space Sci. Rev.*, 3, 816  
Press, W. H., Teukolsky S. A., Vetterling W. T., & Flannery B. P. 1992, *Numerical Recipes in Fortran* (2d ed.; Cambridge: Cambridge Univ. Press)  
Raymond, J. C., & Doyle, J. G. 1981, *ApJ*, 247, 686  
Reeves, E. M., Huber, M. C., & Timothy, J. G. 1977, *Appl. Opt.*, 16, 837  
Thompson, A. M. 1991, in *Integral Intensity Inversion Techniques: a Study in Preparation for the SOHO Mission*, ed. A. M. Thompson & R. A. Harrison (Oxon: RAL), RAL91-092  
Turchin, V. F., Kazlov, V. P., & Malkevich, M. S. 1971, *Soviet Phys. Uspekhi*, 13, 61  
Vernazza, J. E., & Reeves, E. M. 1978, *ApJS*, 37, 485